nature COMMUNICATIONS

ARTICLE

Received 7 Dec 2015 | Accepted 22 Mar 2016 | Published 20 Apr 2016

DOI: 10.1038/ncomms11404 OPEN

A nine-atom rhodium–aluminum oxide cluster oxidizes five carbon monoxide molecules

Xiao-Na Li[1], Hua-Min Zhang[1], Zhen Yuan[1,2] & Sheng-Gui He[1]

Noble metals can promote the direct participation of lattice oxygen of very stable oxide materials such as aluminum oxide, to oxidize reactant molecules, while the fundamental mechanism of noble metal catalysis is elusive. Here we report that a single atom of rhodium, a powerful noble metal catalyst, can promote the transfer of five oxygen atoms to oxidize carbon monoxide from a nine-atom rhodium–aluminum oxide cluster. This is a sharp improvement in the field of cluster science where the transfer of at most two oxygen atoms from a doped cluster is more commonly observed. Rhodium functions not only as the preferred trapping site to anchor and oxidize carbon monoxide by the oxygen atoms in direct connection with rhodium but also the primarily oxidative centre to accumulate the large amounts of electrons and the polarity of rhodium is ultimately transformed from positive to negative.

[1] Beijing National Laboratory for Molecular Sciences, State Key Laboratory for Structural Chemistry of Unstable and Stable Species, Institute of Chemistry, Chinese Academy of Sciences, Zhongguancun North First Street 2, Beijing 100190, China. [2] University of Chinese Academy of Sciences, Beijing 100049, China. Correspondence and requests for materials should be addressed to S.-G.H. (email: shengguihe@iccas.ac.cn).

Oxide-supported rhodium (Rh) exhibits extraordinary catalytic activity in a large number of reactions[1–9] such as the oxidation of carbon monoxide (CO)[1–3,7], carbon dioxide methanation[6], partial oxidation of methane to syngas[4,5,8,9] and so on. It has been reported that trace amounts of Rh can promote direct participation of lattice oxygen of chemically very inert supports such as aluminum oxide (Al_2O_3), to oxidize reactant molecules[4,5,9], while the fundamental mechanism is elusive. Exploring the function of Rh in invoking the lattice oxygen of oxide support is of great importance to understand heterogeneous catalysis but remains a big challenge because of the structure complexity of bulk material.

Atomic clusters are considered as the intermediate matter to bridge atoms and their bulk counterpart[10], and can be ideal models for active sites of condensed-phase system. Cluster reactions[11–17] can be studied under isolated conditions to provide the mechanistic insights of elementary steps in the related condensed-phase systems. Important findings such as spin conservation[13] and the complementary active sites[15] have been revealed by studying the reactions of aluminum clusters with molecular O_2 and water, respectively. The oxygen atom transfer (OAT) from metal oxide clusters to small molecules is one type of extensively studied reactions[12,18,19]. Noble metal-doped heteronuclear oxide clusters[20] are being actively studied to understand the mechanistic nature of supported catalysts in the OAT reactions such as CO oxidation, an important model reaction in heterogeneous processes[21] and its wide applications in air purification. Au and Pt atoms have been emphasized to be crucial, to promote significantly the efficiency of OAT in CO oxidation[22–26]. However, each of the reported Au or Pt-doped clusters such as $AuAl_3O_5^+$ and $PtAl_3O_7^-$ can transfer at most two oxygen atoms to oxidize CO (refs 22–26). Here we report that a single Rh atom can unexpectedly promote the transfer of five oxygen atoms to oxidize CO from a nine-atom cluster $RhAl_2O_6^+$, which produces the oxygen very deficient species $RhAl_2O^+$. In contrast, reported homonuclear aluminum oxide clusters ($Al_xO_y^{\pm}$)[26,27] can deliver only one oxygen atom to CO and these reactive clusters such as $Al_2O_3^+$ and $Al_4O_7^-$ are all oxygen-rich species. Identification of multiple OAT from a single Rh-atom-doped cluster to reactant molecules is an important step to understand the participation of lattice oxygen promoted by noble metals. This gas-phase study that a nine-atom rhodium–aluminum oxide cluster oxidizes five CO molecules is a sharp improvement in the field of cluster science and provides a strictly molecular level understanding of the fundamental mechanism of noble metal catalysis in the related condensed phase.

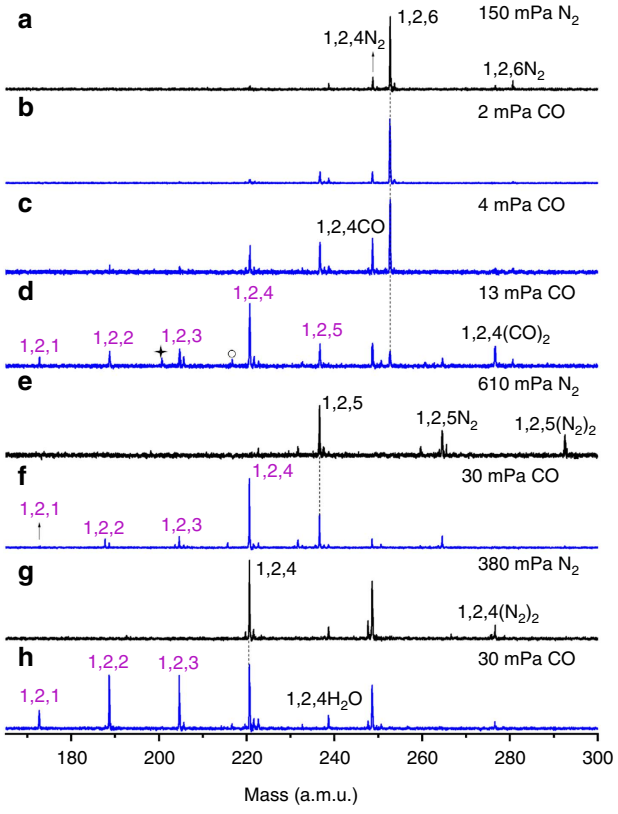

Figure 1 | Reactivity of $RhAl_2O_{4-6}^+$ clusters with CO. Time-of-flight mass spectra for reactions of mass selected $RhAl_2O_{4-6}^+$ with N_2 (**a**,**e**,**g**) and CO (**b**–**d**,**f**,**h**) are shown. Peaks marked with asterisk and hollow circle in **d** are CO adsorption products of $RhAl_2OCO^+$ and $RhAl_2O_2CO^+$, respectively. $Rh_xAl_yO_z^+$ and $Rh_xAl_yO_zX^+$ ($X = N_2$, CO and H_2O) species are labeled as *x,y,z* and *x,y,zX*, respectively. Signal $1,2,4H_2O$ in **h** is due to the residual water in the gas handling system. The time periods for reactions $RhAl_2O_6^+ + CO$, $RhAl_2O_5^+ + CO$ and $RhAl_2O_4^+ + CO$ were about 1.1, 0.7 and 0.6 ms, respectively. The reactant gas pressures are shown in mPa.

Results

Reactivity of rhodium–aluminum oxide clusters with CO. The $RhAl_2O_m^+$ ($m = 2$–6) cluster ions were generated by laser ablation of a mixed-metal disk compressed with Rh and Al powders. The generated $RhAl_2O_m^+$ cluster ions were mass-selected, cooled and then interacted with N_2 and CO in an ion trap reactor, as shown in Figs 1 and 2. On the interaction of $RhAl_2O_6^+$ with 150 mPa N_2 (Fig. 1a), weak N_2 adsorption ($RhAl_2O_6N_2^+$) and N_2/O_2 exchange ($RhAl_2O_4N_2^+$) products were generated. Generation of $RhAl_2O_4N_2^+$ suggests the possible presence of superoxide ($O_2^{-\bullet}$) or peroxide (O_2^{2-}) unit in $RhAl_2O_6^+$ ($RhAl_2O_6^+ + N_2 \rightarrow RhAl_2O_4N_2^+ + O_2$). In sharp contrast, on the interaction of $RhAl_2O_6^+$ with CO (Fig. 1b–d), a series of products, from $RhAl_2O_5^+$ to $RhAl_2O^+$, were generated gradually with the increase of CO partial pressure from 2 to 13 mPa. Signals $RhAl_2O_{1-5}^+$ did not appear on the interaction of $RhAl_2O_6^+$ with even high pressure N_2 (Fig. 1a). Additional experimental techniques such as multiphoton ionization[28,29] employing pulsed lasers are required to observe the neutral CO_2 molecules. However, N_2 experiment in Fig. 1a also indicates that products $RhAl_2O_{1-5}^+$ are due to the chemical reactions of $RhAl_2O_6^+$ with CO rather than collision-induced dissociation and $RhAl_2O_6^+$ may oxidize five CO molecules consecutively (equation (1)).

$$RhAl_2O_m^+ + CO \rightarrow RhAl_2O_{m-1}^+ + CO_2 \ (m = 6-2) \quad (1)$$

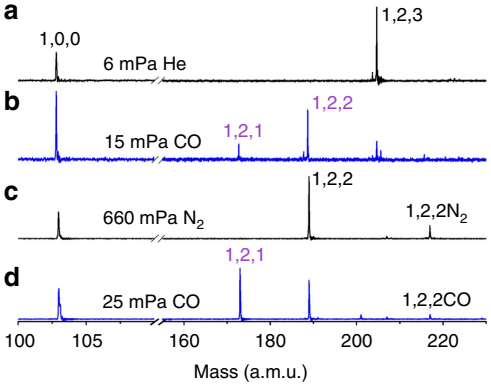

Figure 2 | Reactivity of $RhAl_2O_{2-3}^+$ clusters with CO. Time-of-flight mass spectra for reactions of mass selected $RhAl_2O_{2-3}^+$ with He (**a**), N_2 (**c**) and CO (**b**,**d**) are shown. The time period was ~0.6 ms for both reactions.

The strong signals that can be assigned as $RhAl_2O_4CO^+$ and $RhAl_2O_4(CO)_2^+$ (Fig. 1a–d) on the interaction of $RhAl_2O_6^+$ with CO indicate the displacement of the O–O unit in $RhAl_2O_6^+$ by CO, which is more facile than N_2 displacement (Fig. 1a), and further demonstrates the presence of $O_2^{-\bullet}$ or O_2^{2-} unit in $RhAl_2O_6^+$. Each of the cluster source generated $RhAl_2O_m^+$ ($m=5-2$) clusters could also react with CO to generate products, from $RhAl_2O_{m-1}^+$ to $RhAl_2O^+$ (Figs 1f,h and 2b,d). This provides convincing evidence that $RhAl_2O_6^+$ can indeed oxidize five CO molecules consecutively. The pseudo-first-order rate constants (k_1, in unit of 10^{-10} cm^3 per molecule per second) on the interaction of $RhAl_2O_m^+$ ($m=6$–2) cluster ions with CO can be well fitted (Fig. 3) and the determined rate constants are presented in Supplementary Table 1. The rate constants for the reactions of the cluster source generated $RhAl_2O_m^+$ ($m=6$–2) with CO are 4.9 ± 1.5 ($m=6$), 6.2 ± 1.9 ($m=5$), 1.6 ± 0.5 ($m=4$), 6.9 ± 2.0 ($m=3$) and 2.4 ± 0.7 ($m=2$), which correspond to the reaction efficiencies[30] of about (37 ± 11)%, (47 ± 14)%, (13 ± 4)%, (54 ± 16)% and (19 ± 6)%, respectively. Furthermore, we note that the clusters with odd number of oxygen atoms such as $RhAl_2O_5^+$ are more reactive towards CO oxidation than clusters with even number of oxygen atoms such as $RhAl_2O_6^+$.

Reaction mechanism. The density functional theory calculated thermodynamic data for CO oxidation by $RhAl_2O_m^+$ ($m=2$–6) are shown in Fig. 4. The overall oxidation ($RhAl_2O_6^+ + 5CO \rightarrow RhAl_2O^+ + 5CO_2$) is highly exothermic ($-9.00$ eV). The low-lying energy isomers of clusters $RhAl_2O_m^+$ ($m=6$–1) are provided in Supplementary Figs 1–6. The lowest energy isomer of $RhAl_2O_6^+$ is in the triplet spin state (Supplementary Fig. 1) and contains a superoxide $O_2^{-\bullet}$ unit (O–O bond: 137 pm; Fig. 5). The existence of $O_2^{-\bullet}$ unit in $RhAl_2O_6^+$ is consistent with the appearance of $RhAl_2O_4N_2^+$ and $RhAl_2O_4CO^+$ (or $RhAl_2O_4(CO)_2^+$) on the interaction of $RhAl_2O_6^+$ with N_2 and CO (Fig. 1a–d), respectively. Supplementary Figs 7 and 8 show that the Al-site adsorption contributes to the displacement of the $O_2^{-\bullet}$ unit in $RhAl_2O_6^+$ by N_2 or CO and both reactions are calculated to be thermodynamically and kinetically favourable, and CO displacement is more facile than N_2 displacement. This is consistent with the relatively higher intensity of $RhAl_2O_4CO^+$ (or $RhAl_2O_4(CO)_2^+$) than $RhAl_2O_4N_2^+$ observed in the experiment (Fig. 1a–d). The positively charged Rh in $RhAl_2O_6^+$ (natural charge: $+1.14$ e) can trap CO tightly at the first step (I1, $\Delta H_0=-1.49$ eV; Fig. 5) and then the oxidation of CO (I1 → TS1 → I2) by the highly reactive atomic oxygen radical

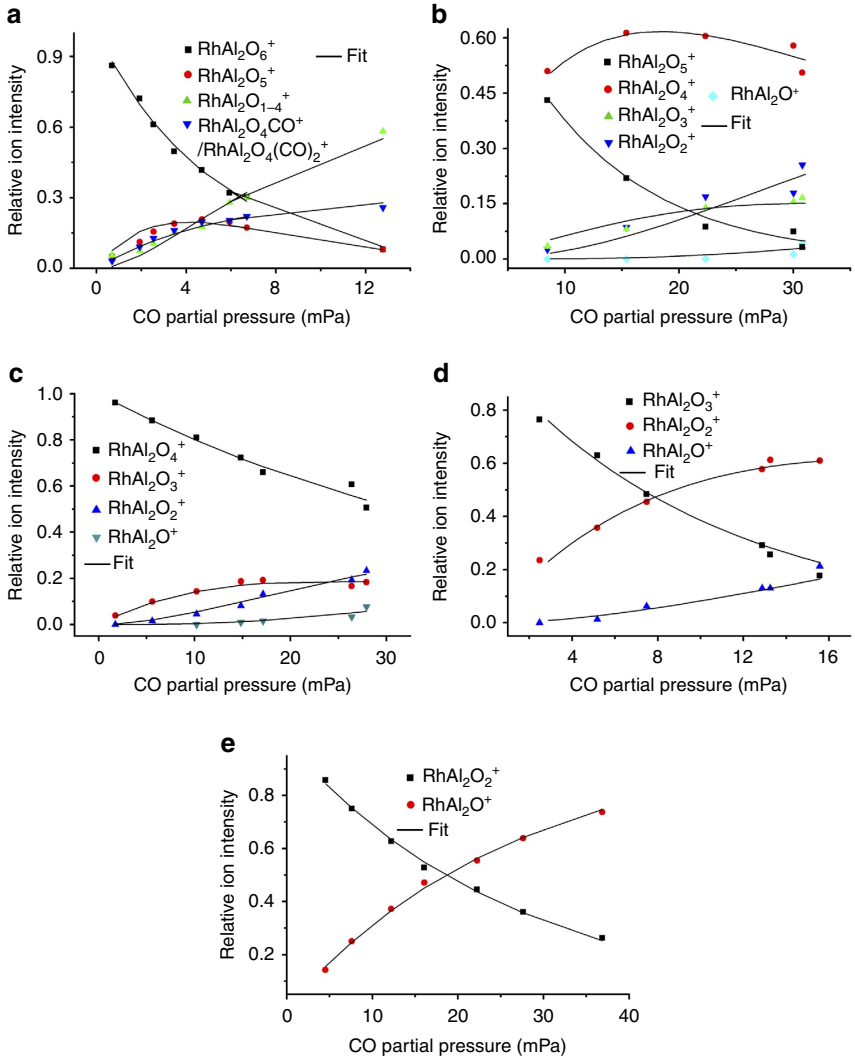

Figure 3 | Reaction kinetics. Variation of ion intensities with respect to the partial pressures of CO in $RhAl_2O_m^+$ ($m=6-2$) + CO are shown (**a**–**e**). The solid lines are fitted to the experimental data points by the least-square procedure. The Rh^+ (1,0,0) ions (Fig. 2) are mostly generated during cooling of the $RhAl_2O_3^+$ and $RhAl_2O_2^+$ cluster ions through collisions with He gas in the ion trap reactor; thus, the ion intensity of Rh^+ (nearly independent on the CO partial pressure) is excluded in the fitting. See Supplementary Table 1 for details of the determined rate constant values.

anion $O^{-\bullet}$ (ref. 31) takes place. Direct CO oxidation by the $O_2^{-\bullet}$ unit has to suffer from a positive barrier of 0.03 eV, which is much less favourable than the oxidation by $O^{-\bullet}$. The Rh atom in product $RhAl_2O_5^+$ (denoted as $^PRhAl_2O_5^+$, the structure of which is different from the lowest energy structure; Supplementary Fig. 2) can capture another CO tightly (I3, binding energy of −2.18 eV). Formation of the bent CO_2 is the bottleneck (I3→TS2→I4) for CO oxidation by $^PRhAl_2O_5^+$. This step is to subject to a barrier of 1.26 eV. The subsequent steps follow a nearly downhill pathway characterized by small barriers to yield $RhAl_2O_4^+$ and CO_2 (Supplementary Fig. 9). Furthermore, theoretical calculations show that the energy of the critical transition state for reaction $RhAl_2O_5^+ + CO$ (−0.47 eV; Supplementary Fig. 10) is lower with respect to that for reaction $RhAl_2O_6^+ + CO$ (TS1, −0.37 eV; Fig. 5). This can well interpret the more reactive behaviour of the cluster source-generated $RhAl_2O_5^+$ than $RhAl_2O_6^+$ in the experiment.

The key step for the transfer of five oxygen atoms from $RhAl_2O_6^+$ to CO lies in the facile dissociation of the $O_2^{-\bullet}$ unit in $^PRhAl_2O_5^+$. Dissociation of the chemically adsorbed molecular O_2 (superoxide $O_2^{-\bullet}$ or peroxide O_2^{2-}) is often considered to be the crucial step in oxidation reactions[32]. Recent gas-phase studies indicated that a single Au atom in $AuTi_3O_8^-$ [22] is not enough to promote the dissociation of the O_2^{2-} unit, while the Au dimer in $Au_2VO_4^-$ can promote O_2^{2-} unit dissociation or direct participation in CO oxidation[25]. In this study, a single Rh atom in $^PRhAl_2O_5^+$ can promote the dissociation of the $O_2^{-\bullet}$ unit and the process is much more favourable than CO_2 desorption (Fig. 5). This is rationalized by the strong Rh–C multiple bonds (5.97 eV)[33] and the strong Rh–O bond (4.16 eV)[34]. Thus, the Al–$O_2^{-\bullet}$ unit in I4 can approach the Rh atom favourably to form structure Al–O_2^{2-}···Rh–CO_2 in I5. The elongation of the O–O bond from 137 pm in I4 to 147 pm in I5 is a good indicator for the activation of the superoxide $O_2^{-\bullet}$ to peroxide O_2^{2-} unit. The structure of I5 is crucial to induce further electron flowing into the O_2^{2-} unit from both of the Rh atom and the CO_2 unit (Fig. 5), and then the O_2^{2-} unit can be dissociated favourably to produce O^{2-}–Al–O^{2-}–Rh–CO_2 (I5→TS4→I6). Direct oxidation of CO by the $O_2^{-\bullet}$ unit in $^PRhAl_2O_5^+$ (Supplementary Fig. 9) is less favourable than the pathway in Fig. 5. This is consistent with previous study that instead of the direct participation in CO oxidation, molecular oxygen adsorbs at the interface between the oxygen vacancy and the single Rh site and then is followed by facile dissociation[35]. Release of three additional oxygen atoms from the resulting $RhAl_2O_4^+$ to CO are calculated to be thermodynamically and kinetically favourable (Supplementary Figs 11–13). In each of these OAT steps, Rh atom functions as the preferred trapping site to anchor CO and then delivers CO for oxidation by the oxygen atoms in direct connection with Rh. The theoretical calculations well interpret the unique reactivity of $RhAl_2O_6^+$ observed in the experiment.

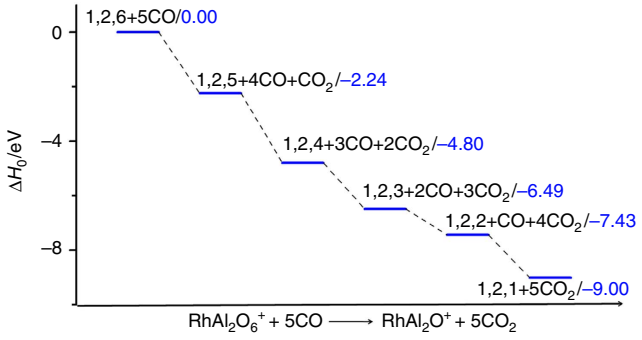

Figure 4 | Reaction thermodynamics. Density functional theory (DFT)-calculated thermodynamic data for CO oxidation by $RhAl_2O_{2\text{-}6}^+$. The energies are zero-point vibration-corrected in unit of eV.

Discussion

Metal-mediated OAT reaction is usually accompanied with the reduction of central metal by electrons that are stored originally in the removed oxygen atoms[36] (equation (2)).

$$M^{n+}O_x + R \rightarrow M^{(n-2)+}O_{x-1} + RO \qquad (2)$$

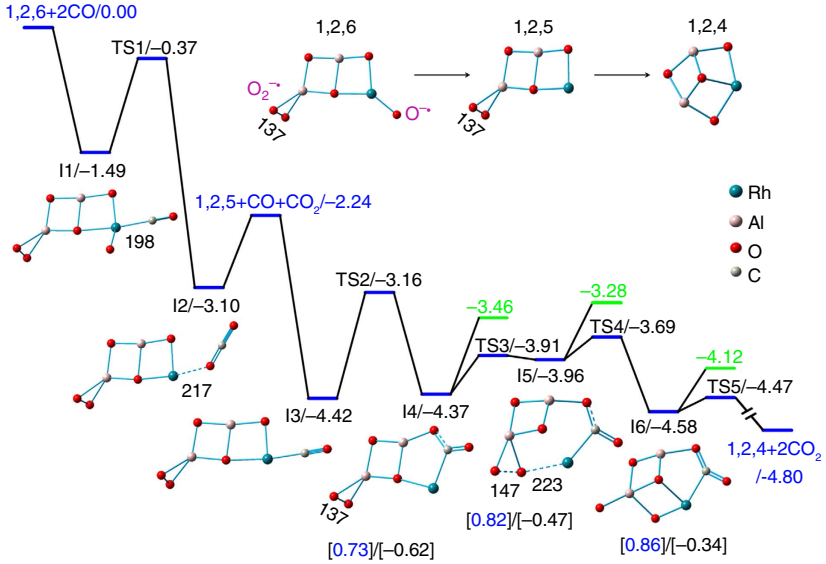

Figure 5 | Structures and reaction mechanisms. Density functional theory (DFT)-calculated potential energy profiles for the oxidation of the first two CO molecules by $RhAl_2O_6^+$. The lowest energy structure of $RhAl_2O_6^+$ (1,2,6) and the products $^PRhAl_2O_5^+$ (1,2,5) and $RhAl_2O_4^+$ (1,2,4) are provided. Symbols $O_2^{-\bullet}$ and $O^{-\bullet}$ denote superoxide and atomic oxygen radical species, respectively. The relative energies for intermediates (I1–I6) and transition states (TS1–TS5) are in unit of eV. Structures of I1–I6 are shown. Bond lengths are given in pm. The values in green show the relative energies for direct CO_2 desorption from I4 to I6. The values in the square brackets show the natural charges on Rh (blue) and CO_2 unit (black). See also Supplementary Figs 9–13 for more information.

The positively charged metal centre is crucial to provide not only the characteristic site for the adsorption of CO (ref. 37) but also the oxidative centre to accept electrons. Recent gas-phase studies highlighted that the cleavage of Au–O bond and the formation of Au–*M* bond (*M* = Al, V, Ti, and Fe) is of great importance in CO oxidation by Au-doped clusters[22–25]. However, each of the Au-doped clusters can oxidize only one or at most two CO molecules and then the polarity conversion of Au atom from positive to negative takes place because of the formation of the reductive Au–*M* bond. In sharp contrast, natural charge analysis demonstrates that after the transfer of four oxygen atoms from $RhAl_2O_6^+$ to CO, the Rh atom is still positively charged (+0.53*e*, Fig. 6) in product $RhAl_2O_2^+$, which can also oxidize a CO molecule. The natural charge on Rh atom is decreased from +1.14*e* in $RhAl_2O_6^+$ to +1.00*e* in $^{P}RhAl_2O_5^+$ after the oxidation of the first CO. In this step, Rh acts as the primary centre to accumulate the electron that is localized originally on $O^{-\bullet}$ radical, as shown from the change of spin density distribution, $RhAl_2O_6^+$ versus $^{P}RhAl_2O_5^+$. However, the Rh atom is re-oxidized in product $RhAl_2O_4^+$ (+1.15*e*) after the oxidation of the second CO due to the dissociation of the $O_2^{-\bullet}$ unit (I4→I5→I6; Fig. 5). This step is crucial to recover the oxidative reactivity of Rh. *In situ* Raman spectroscopic study also demonstrated that supported Rh oxide can oxidize CO and then the Rh oxide is subsequently re-oxidized by the oxygen atoms from oxide support[7]. This phenomenon can be traced back to the well-fitting strength of Rh–O bond (4.16 eV)[34], which is strong enough to promote the dissociation of the $O_2^{-\bullet}$ unit in $^{P}RhAl_2O_5^+$ and prevent the formation of the reductive Rh–Al bond (3.26 eV, by theoretical calculation) in $RhAl_2O_{2-6}^+$ but at the same time is relatively weak to deliver oxygen atoms to oxidize CO (O–CO: 5.52 eV)[38]. Previous studies show that Rh prefers to coordinate not only with the surface oxygen atoms but also the subsurface oxygen in oxide support[35]. The strong Rh–O bond inhibits the migration of Rh atom to the oxygen vacancy and remains positively charged. Using high-resolution *in situ* X-ray diffraction and transmission electron microscopy, Stierle and colleagues[1] reported the reversible and oxygen-induced shape transformation of Rh nanoparticles by the formation of O–Rh–O surface oxide during the cycle of catalytic CO oxidation. In contrast, the stronger Au–M (Au–Al = 3.37 eV (ref. 39), Au–V = 2.49 eV (ref. 38) and Au–Ti = 2.56 eV (by theoretical calculation)) than Au–O bond (2.27 eV)[34] facilitates the formation of the reductive Au–M bond after the oxidation of only one or two CO molecules.

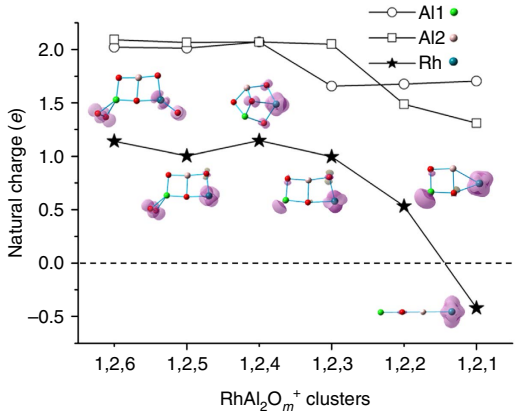

Figure 6 | Natural charge. Density functional theory (DFT)-calculated natural charges (e) on the Rh atom and Al atoms in $RhAl_2O_{1-6}^+$. The spin density distributions on individual atoms are shown in the purple isosurfaces.

The negatively charged Rh has been theoretically predicted[40] and experimentally postulated[41]. The $RhAl_2O^+$ cluster is a linear structure (Al–O–Al–Rh) and the single oxygen atom is sandwiched between two Al atoms. This structure with triplet spin state has been confirmed to be the lowest energy isomer of $RhAl_2O^+$ by more accurate CCSD(T) calculation (Supplementary Fig. 6). The two unpaired electrons are mainly localized on the Rh atom (~1.83 μ_B, Fig. 6), indicating that such Rh atom can be considered to be Rh^{-1} ($4d^9 5s^1$). The electron configuration calculations ($4d^{8.75}5s^{0.64}5p^{0.03}$) provide solid evidence for the negatively charged Rh in $RhAl_2O^+$. Thus, the oxidation state of Rh changes from +2.5 in $RhAl_2O_6^+$ to −1 in $RhAl_2O^+$ (calculated based on the distribution of spin density; Fig. 6) during the transfer of five oxygen atoms from $RhAl_2O_6^+$ to CO. This rather large range of Rh oxidation state changes in chemical reactions has rarely been reported (the Au oxidation state changes from +1 to −1), covering from cationic to anionic, and it is the driving force to accumulate the electrons that are stored originally in the released oxygen atoms and promotes the unique oxidative reactions to proceed.

In conclusion, we have demonstrated that a single atom of Rh can unexpectedly promote the transfer of five oxygen atoms to oxidize CO from a nine-atom cluster $RhAl_2O_6^+$. This study leads a leap ahead towards OAT reactions in the field of cluster science and represents an important step to understand the participation of lattice oxygen promoted by noble metals. The preferable Rh–O rather than the reductive Rh–Al bond formation together with the capability of Rh to accumulate the large amounts of electrons are crucial factors to drive the unique reactions. This gas-phase study reveals the molecular-level origin for the puzzling experimental observation that trace amounts of Rh can promote the reactivity of lattice oxygen of Al_2O_3 (refs 4,5,9), a chemically very inert material.

Methods

Cluster generation and reactivity detection. The $Rh_xAl_yO_z^+$ cluster ions were generated by laser ablation of a mixed-metal disk compressed with Rh and Al powders (molar radio Rh/Al = 1/1) in the presence of O_2 (0.4%) seeded in a He carrier gas with a backing pressure of 6.0 standard atmospheres. The cluster ions of interest were mass selected using a quadrupole mass filter and then entered into a linear ion trap (LIT) reactor, where they were cooled by collisions with a pulse of He gas and then interacted with a pulse of 5% (for reactions $RhAl_2O_m^+$ (*m* = 2–5) + CO) or 2% (for reaction $RhAl_2O_6^+$ + CO) CO seeded in He for around 0.6 ~ 1.1 ms. The temperature of cooling gas (He), reactant gases (CO or N_2) and the LIT reactor was around 298 K. The cluster ions ejected from the LIT were detected by a reflector time-of-flight mass spectrometer. The details of running the time-of-flight mass spectrometer[42], quadrupole mass filter[43] and the LIT[44] can be found in our previous works.

Rate constant fitting. Equation (3) was used to determine the pseudo-first-order rate constants (k_1) of cluster reactions in an ion trap reactor[44], in which I_R is the signal intensity of the reactant cluster ions, I_T is the total ion intensity including product ion contribution, k_B is the Boltzmann constant, *T* is the temperature (~298 K), t_R is the reaction time and *P* is the effective pressure of the reactant gas in the ion trap reactor.

$$\ln\frac{I_R}{I_T} = -k_1\frac{P}{k_B T}t_R \quad (3)$$

To calculate the reaction efficiencies (the possibilities of reaction on each collision), the collision rate constants were calculated on the basis of the surface charge capture model developed in the literature[30]. It is noteworthy that for reaction $RhAl_2O_5^+$ + CO, the relative ion intensity of $RhAl_2O_5^+$ is the reactive component generated in the experiment and the unreactive component is not included. The unreactive component of $RhAl_2O_5^+$ could be well-fitted by equation (4)[45].

$$I_R = x_{inert} + (1 - x_{inert}) \times \exp(-k_1\frac{P}{k_B T}t_R) \quad (4)$$

in which x_{inert} is the relative intensity of the unreactive component of $RhAl_2O_5^+$ and k_1 is the pseudo-first-order rate constant of the reactive component of $RhAl_2O_5^+$. The x_{inert} was determined to be about 12%, indicating that the experimentally generated $RhAl_2O_5^+$ may have isomers that are not or less reactive with CO.

Computational details. Density functional theory calculations using the Gaussian 09 (ref. 46) programme were carried out to investigate the mechanistic details on the oxidation of five CO molecules by a nine-atom rhodium–aluminum oxide cluster ($RhAl_2O_6^+$). To find an appropriate functional for the Rh–Al–O system, the bond dissociation energies of Rh–O, Rh–C, Al–O, O–O, Rh–Al and O–CO were computed by various functionals and compared with available experimental data (Supplementary Table 2). It turns out that M06L[47] was the best overall; thus, the results by M06L were given throughout the work. The TZVP basis set[48] for Al, C and O atoms and a D95V basis set[49] combined with the Stuttgart/Dresden relativistic effective core potential (denoted as SDD in Gaussian software) for Rh atom were used in all the calculations. A Fortran code based on a genetic algorithm[50] was used to generate initial guess structures of $RhAl_2O_{1-6}^+$. The reaction mechanisms were studied for $RhAl_2O_6^+ + 5CO \rightarrow RhAl_2O^+ + 5CO_2$. The relaxed potential energy surface scan was used extensively to obtain good guess structures for intermediates and transition states along the pathways. The transition states were optimized using the Berny algorithm[51]. Intrinsic reaction coordinate calculations[52,53] were performed so that each transition state connects two appropriate local minima. Vibrational frequency calculations were carried out to check that intermediates and transition state have zero and only one imaginary frequency, respectively.

References

1. Nolte, P. *et al.* Shape changes of supported Rh nanoparticles during oxidation and reduction cycles. *Science* **321,** 1654–1658 (2008).
2. Grass, M. E. *et al.* A reactive oxide overlayer on rhodium nanoparticles during CO oxidation and its size dependence studied by in situ ambient-pressure X-ray photoelectron spectroscopy. *Angew. Chem. Int. Ed.* **47,** 8893–8896 (2008).
3. Ligthart, D. A. J. M., van Santen, R. A. & Hensen, E. J. M. Supported rhodium oxide nanoparticles as highly active CO oxidation catalysts. *Angew. Chem. Int. Ed.* **50,** 5306–5310 (2011).
4. Karin, C. B., Wohlrab, S., Rodemerck, U. & Kondratenko, E. V. The tremendous effect of trace amounts of Rh on redox and catalytic properties of CeO_2-TiO_2 and Al_2O_3 in CH_4 partial oxidation. *Catal. Commun.* **18,** 121–125 (2012).
5. Karin, C. B. *et al.* Tailored noble metal nanoparticles on γ-Al_2O_3 for high temperature CH_4 conversion to syngas. *ChemCatChem.* **4,** 1368–1375 (2012).
6. Karelovic, A. & Ruiz, P. Improving the hydrogenation function of Pd/γ-Al_2O_3 catalyst by Rh/γ-Al_2O_3 addition in CO_2 methanation at low temperature. *ACS Catal.* **3,** 2799–2812 (2013).
7. Song, W., Jansen, A. P. J., Degirmenci, V., Ligthart, D. A. J. M. & Hensen, E. J. M. A computational study of the mechanism of CO oxidation by a ceria supported surface rhodium oxide layer. *Chem. Commun.* **49,** 3851–3853 (2013).
8. Duarte, R. B., Krumeich, F. & van Bokhoven, J. A. Structure, activity, and stability of atomically dispersed Rh in methane stream reforming. *ACS Catal.* **4,** 1279–1286 (2014).
9. Kondratenko, V. A., Karin, C. B. & Kondratenko, E. V. Partial oxidation of methane to syngas over γ-Al_2O_3-supported Rh nanoparticles: kinetic and mechanistic origins of size effect on selectivity and activity. *ACS Catal.* **4,** 3136–3144 (2014).
10. Castleman, Jr A. W. & Jena, P. Clusters: a bridge between disciplines. *Proc. Natl Acad. Sci. USA* **103,** 10552–10553 (2006).
11. O'Hair, R. A. J. & Khairallah, G. N. Gas phase ion chemistry of transition metal clusters: production, reactivity, and catalysis. *J. Clust. Sci.* **15,** 331–363 (2004).
12. Böhme, D. K. & Schwarz, H. Gas-phase catalysis by atomic and cluster metal ions: the ultimate single-site catalysts. *Angew. Chem. Int. Ed.* **44,** 2336–2354 (2005).
13. Burgert, R. *et al.* Spin conservation accounts for aluminum cluster anion reactivity pattern with O_2. *Science* **319,** 438–442 (2008).
14. Gong, Y. & Zhou, M. Spectroscopic and theoretical studies of transition metal oxides and dioxygen complexes. *Chem. Rev.* **109,** 6765–6808 (2009).
15. Roach, P. J., Woodward, W. H., Castleman, Jr A. W., Reber, A. C. & Khanna, S. N. Complementary active sites cause size-selective reactivity of aluminum cluster anions with water. *Science* **323,** 492–495 (2009).
16. Lang, S. M. & Bernhardt, T. M. Gas phase metal cluster model systems for heterogeneous catalysis. *Phys. Chem. Chem. Phys.* **14,** 9255–9269 (2012).
17. Asmis, K. R. Structure characterization of metal oxide clusters by vibrational spectroscopy: possibilities and prospects. *Phys. Chem. Chem. Phys.* **14,** 9270–9281 (2012).
18. Blagojevic, V., Orlova, G. & Bohme, D. K. O-atom transport catalysis by atomic cations in the gas phase: reduction of N_2O by CO. *J. Am. Chem. Soc.* **127,** 3545–3555 (2005).
19. Liu, Q. Y. & He, S. G. Oxidation of carbon monoxide on atomic clusters. *Chem. J. Chin. Univ.* **35,** 665–688 (2014).
20. Schwarz, H. Doping effects in cluster-mediated bond activation. *Angew. Chem. Int. Ed.* **54,** 10090–10100 (2015).
21. Freund, H. J., Meijer, G., Scheffler, M., Schlögl, R. & Wolf, M. CO oxidation as prototypical reaction for heterogeneous processes. *Angew. Chem. Int. Ed.* **50,** 10064–10094 (2011).
22. Li, X. N., Yuan, Z. & He, S. G. CO oxidation promoted by gold atoms supported on titanium oxide cluster anions. *J. Am. Chem. Soc.* **136,** 3617–3623 (2014).
23. Li, Z. Y., Yuan, Z., Li, X. N., Zhao, Y. X. & He, S. G. CO oxidation catalyzed by single gold atoms supported on aluminum oxide clusters. *J. Am. Chem. Soc.* **136,** 14307–14313 (2014).
24. Yuan, Z., Li, X. N. & He, S. G. CO oxidation promoted by gold atoms loosely attached in $AuFeO_3^-$ cluster anions. *J. Phys. Chem. Lett.* **5,** 1585–1590 (2014).
25. Wang, L. N. *et al.* CO oxidation promoted by the gold dimer in $Au_2VO_3^-$ and $Au_2VO_4^-$ clusters. *Angew. Chem. Int. Ed.* **54,** 11720–11724 (2015).
26. Li, X. N., Yuan, Z., Meng, J. H., Li, Z. Y. & He, S. G. Catalytic CO oxidation on single Pt-atom doped aluminum oxide clusters: electronegativity-ladder effect. *J. Phys. Chem. C* **119,** 15414–15420 (2015).
27. Johnson, G. E., Tyo, E. C. & Castleman, Jr A. W. Oxidation of CO by aluminum oxide cluster ions in the gas phase. *J. Phys. Chem. A* **112,** 4732–4735 (2008).
28. Li, S., Mirabal, A., Demuth, J., Wöste, L. & Siebert, T. A complete reactant-product analysis of the oxygen transfer reaction in $[V_4O_{11}{\cdot}C_3H_6]^-$: a cluster complex for modeling surface activation and reactivity. *J. Am. Chem. Soc.* **130,** 16832–16833 (2008).
29. Li, S., Demuth, J., Mirabal, A., Wöste, L. & Siebert, T. On the role of thermal activation in selective photochemistry: mechanistic insight into the oxidation of propene on the $V_4O_{11}^-$ cluster. *Phys. Chem. Chem. Phys.* **14,** 148–156 (2012).
30. Kummerlöwe, G. & Beyer, M. K. Rate estimates for collisions of ionic clusters with neutral reactant molecules. *Int. J. Mass Spectrom.* **244,** 84–90 (2005).
31. Ma, J. B. *et al.* Reactivity of atomic oxygen radical anions bound to titania and zirconia nanoparticles in the gas phase: low-temperature oxidation of carbon monoxide. *J. Am. Chem. Soc.* **136,** 2991–2998 (2013).
32. Panov, G. I., Dubkov, K. A. & Starokon, E. V. Active oxygen in selective oxidation catalysis. *Catal. Today* **117,** 148–155 (2006).
33. Shim, I. & Gingerich, K. A. Electronic structure and bonding in the RhC molecule by all-electron ab initio HF-CI calculations and mass spectrometric measurements. *J. Chem. Phys.* **81,** 5937–5944 (1984).
34. Pedley, J. B. & Marshall, E. M. Thermochemical data for gaseous monoxides. *J. Phys. Chem. Ref. Data* **12,** 967–1031 (1983).
35. Song, W., Jansen, A. P. J. & Hensen, E. J. M. A computational study of the influence of the ceria surface termination on the mechanism of CO oxidation of isolated Rh atoms. *Faraday Discuss* **162,** 281–292 (2013).
36. Holm, R. H. Metal-centered oxygen atom transfer reactions. *Chem. Rev.* **87,** 1401–1449 (1987).
37. Guzman, J. & Gates, B. C. Catalysis by supported gold: correlation between catalytic activity for CO oxidation and oxidation states of gold. *J. Am. Chem. Soc.* **126,** 2672–2673 (2004).
38. Luo, Y. P. *Comprehensive Handbook of Chemical Bond Energies*. pp. 9–56 (CRC Press, 2007).
39. Cuthill, A. M., Fabian, D. J. & Shen, S. S. S. Bond dissociation energies of the metallic vapor species aluminum-silver and aluminum-gold measured by Knudsen-Cell mass spectrometry. *J. Phys. Chem.* **77,** 2008–2011 (1973).
40. Gómez, T., Florez, E., Rodriguez, J. A. & Illas, F. Theoretical analysis of the adsorption of late transition-metal atoms on the (001) surface of early transition-meal carbides. *J. Phys. Chem. C* **114,** 1622–1626 (2010).
41. Zafeiratos, S., Nehasil, V. & Ladas, S. X-ray photoelectron spectroscopy study of rhodium particle growth on different alumina surfaces. *Surf. Sci* **433-435,** 612–616 (1999).
42. Wu, X. N., Xu, B., Meng, J. H. & He, S. G. C-H bond activation by nanosized scandium oxide clusters in gas-phase. *Int. J. Mass Spectrom.* **310,** 57–64 (2012).
43. Yuan, Z., Zhao, Y. X., Li, X. N. & He, S. G. Reactions of $V_4O_{10}^+$ cluster ions with simple inorganic and organic molecules. *Int. J. Mass Spectrom.* **354-355,** 105–112 (2013).
44. Yuan, Z. *et al.* Thermal reactions of $(V_2O_5)_nO^-$ ($n=1$–3) cluster anions with ethylene and propylene: oxygen atom transfer versus molecular association. *J. Phys. Chem. C* **118,** 14967–14976 (2014).
45. Li, H. F. *et al.* Methane activation by iron-carbide cluster anions FeC_6^-. *J. Phys. Chem. Lett.* **6,** 2287–2291 (2015).
46. Frisch, M. J. *et al. Gaussian 09, Revision A. 1* (Gaussian, Inc., 2009).
47. Zhao, Y. & Truhlar, D. G. A new local density functional for main-group thermochemistry, transition metal bonding, thermochemical kinetics, and noncovalent interactions. *J. Chem. Phys.* **125,** 194101 (2006).
48. Schäfer, A., Huber, C. & Ahlrichs, R. Fully optimized contracted Gaussian basis sets of triple zeta valence quality for atoms Li to Kr. *J. Chem. Phys.* **100,** 5829–5835 (1994).
49. Andrae, D., Häußermann, U., Dolg, M., Stoll, H. & Preuß, H. Energy-adjusted ab initio pseudopotentials for the second and trird row transition elements. *Theor. Chim. Acta* **77,** 123–141 (1990).
50. Ding, X. L., Li, Z. Y., Meng, J. H., Zhao, Y. X. & He, S. G. Density-functional global optimization of $(La_2O_3)_n$ clusters. *J. Chem. Phys.* **137,** 214311 (2012).

51. Schlegel, H. B. Optimization of equilibrium geometries and transition structures. *J. Comput. Chem.* **3,** 214–218 (1982).
52. Gonzalez, C. & Schlegel, H. B. An improved algorithm for reaction path following. *J. Chem. Phys.* **90,** 2154–2161 (1989).
53. Gonzalez, C. & Schlegel, H. B. Reaction path following in mass-weighted internal coordinates. *J. Phys. Chem.* **94,** 5523–5527 (1990).

Acknowledgements

This work was financially supported by the National Natural Science Foundation of China (Nos 21303215, 21325314, 21273247 and 21573246) and the Major Research Plan of China (No. 2013CB834603).

Author contributions

The original manuscript, figures, tables and the Supplementary Materials were prepared by X.-N.L. The theoretical calculations were prepared by H.-M.Z. and X.-N.L. The experimental data were prepared by Z.Y. and H.-M.Z. S.-G.H. provided the original idea, helpful discussions and the contribution in the manuscript revision.

Additional information

Supplementary Information accompanies this paper at http://www.nature.com/naturecommunications

Competing financial interests: The authors declare no competing financial interests.

Reprints and permission information is available online at http://npg.nature.com/reprintsandpermissions/

How to cite this article: Li, X.-N. *et al.* A nine-atom rhodium–aluminum oxide cluster oxidizes five carbon monoxide molecules. *Nat. Commun.* 7:11404 doi: 10.1038/ncomms11404 (2016).